Inorganic Chemistry

ARTICLE

pubs.acs.org/IC

How To Explain the Difficulties in the Coffinite Synthesis from the Study of Uranothorite?

D. T. Costin,[†] A. Mesbah,[†] N. Clavier,*[,†] N. Dacheux,[†] C. Poinssot,[‡] S. Szenknect,[†] and J. Ravaux[†]

[†]ICSM, UMR 5257 CEA/CNRS/UM2/ENSCM, Site de Marcoule — Bât. 426, BP 17171, 30207 Bagnols/Cèze cedex, France

[‡]CEA, Nuclear Energy Division, DEN/DRCP/DIR, CEA Marcoule — Bât. 400, BP 17171, 30207 Bagnols/Cèze cedex, France

Supporting Information

ABSTRACT: The preparation of $Th_{1-x}U_xSiO_4$ uranothorite solid solutions was successfully undertaken under hydrothermal conditions (T = 250 °C). From XRD and EDS characterization, the formation of a complete solid solution between x = 0 (thorite) and x = 0.8 was evidenced. Nevertheless, additional $(Th,U)O_2$ dioxide and amorphous silica were systematically observed for the highest uranium mole loadings. The influence of kinetics parameters was then studied to avoid the formation of such side products. The variation of the synthesis duration allowed us to point out the initial formation of oxide phases then their evolution to a silicate phase through a dissolution/precipitation process close to that already described as coffinitization. Also, the uranium mole loading initially considered was found to significantly influence the kinetics of reaction, as this latter strongly slows down for x > 0.3. Under these conditions, the difficulties frequently reported in the literature for the synthesis of pure $USiO_4$ coffinite were assigned to a kinetic hindering associated with the coffinitization reaction.

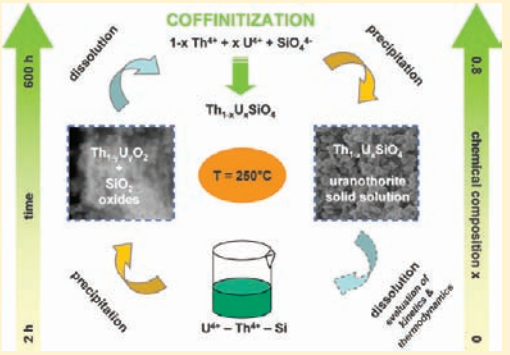

1. INTRODUCTION

High level radioactive waste storage or a nuclear spent fuel repository is currently anticipated to be the standard option in managing the final waste generated in the back-end of the nuclear fuel cycle. Particularly, an underground repository was defined by French law as the standard option for confining the high activity and long-lived fission products and minor actinides elements.[1,2] It is thus important to understand and simulate the behavior of the various radionuclides considered during the evolution of such a site, in particular after the long-term degradation of various confinement barriers and subsequent radwaste leaching. Under these conditions, the kinetics of dissolution as well as the nature of the phases controlling the concentration of radioactive elements in solution through thermodynamics equilibria must be considered carefully.

As many potential host rocks exhibit reducing conditions associated with a silica-rich environment,[3] the concentration of uranium in the direct environment could be controlled by the precipitation of uranium(IV) silicate, known as $USiO_4$ coffinite,[4] depending on the relative stability of coffinite and uraninite. Such a reaction, called coffinitization, was already described in the literature to occur in several natural sites like Oklo reactor (Gabon)[5] or Cigar Lake (Canada):[6]

$$UO_{2+x} + H_4SiO_{4(aq)} \rightleftarrows USiO_4.2H_2O + 0.5xO_2\uparrow \quad (1)$$

The natural presence of coffinite was also reported in various uranium ore deposits all around the world.[7−9] Nevertheless, very few reliable thermodynamic data related to coffinite formation or solubility are available in the literature,[10−13] probably due to the persistent difficulties encountered in the preparation of pure and single-phase $USiO_4$ samples. Indeed, if a large amount of the literature was dedicated to the synthesis of isostructural zircon,[14−16] hafnon,[17,18] or thorite,[19−22] only a few authors reported the successful preparation of coffinite.

Fuchs and Hoekstra were the first to report the synthesis of $USiO_4$ by using a precipitation route under hydrothermal conditions (T = 250 °C, t = 1 day).[23] Nevertheless, UO_2 or SiO_2 were frequently observed as secondary phases, and the pH of the initial mixture was pointed out as a key parameter. This protocol was further adapted to reach single-phase compounds, especially by controlling the surrounding atmosphere to ensure the tetrapositive oxidation state of uranium.[24,25] Nevertheless, all of the methods proposed appeared hardly reproducible since different authors failed to obtain coffinite under the same conditions[26] or did not clearly evidence its formation.[27,28] Moreover, the products were never pure coffinite but rather a mixture of coffinite and uraninite.

On the other hand, several attempts were also made through dry chemistry processes or sol−gel chemistry. In the first case, a mixture of UO_2 and SiO_2 was encapsulated in a platinum container then heated between 250 and 300 °C under a pressure of 50−100 MPa and using a Si/SiO redox buffer.[29] The second

Received: August 3, 2011
Published: September 29, 2011

method was based on the preparation of gelatinous mixtures of $UO_2(NO_3)_2 \cdot 6H_2O$, TEOS, and NH_4OH.[30] These latter were then heated in platinum capsules under hydrothermal conditions (T = 395 °C, P = 500 bar). For both methods, the temperature range was limited by the expected decomposition of coffinite into UO_2 and SiO_2 above 500−600 °C.[31] Under these conditions, no reliable proof arguing for the formation of coffinite was provided by the authors.

Since the direct determination of thermodynamic data requires pure and single phase compounds, indirect methods involving the solubility of $Th_{1-x}U_xSiO_4$ samples should be envisaged for the evaluation of solubility constants of coffinite. Indeed, such data could be reached by means of a solid solution approach based on the study of $Th_{1-x}U_xSiO_4$ samples.[1]

This work was thus devoted to the preparation of synthetic uranothorite solid solutions as a first step before the acquisition of thermodynamic data. The formation of $Th_{1-x}U_xSiO_4$ uranothorite occurring through direct substitution on the cation site was often observed in natural samples.[9,33−35] Nevertheless, this substitution was poorly described in terms of structural modifications in the literature,[36,37] either for synthetic or geological samples. Associated XRD data remain scarce compared to other systems involving actinides in zircon-type structures such as $(Zr,Th)SiO_4$, $(Zr,U)SiO_4$, or $(Zr,Pu)SiO_4$ solid solutions,[38−41] probably due to the metamict/amorphous state of the uranothorite samples.

A complete $Th_{1-x}U_xSiO_4$ series was then prepared through hydrothermal synthesis then fully characterized from a structural and microstructural point of view. The formation of a complete solid solution between thorite and coffinite end members was then discussed in light of the unit cell parameters determined from synthetic samples. Moreover, particular attention was paid to the influence of kinetics on the reaction mechanism in order to supply possible explanations on the persistent difficulties encountered during attempts to prepare pure and single phase coffinite samples.

2. EXPERIMENTAL SECTION

2.1. Chemicals and Synthesis Procedure. All of the reagents used, including thorium nitrate hydrate, were of analytical grade and supplied by Sigma-Aldrich, except uranium tetrachloride solutions. The preparation of uranium tetrachloride was performed by dissolving uranium metal in hydrochloric acid. The metal pieces were first washed in 2 M HCl to eliminate eventual oxide traces present at the surface, rinsed with water and ethanol, and finally dissolved in 6 M HCl. The uranium concentration of the final solution was estimated to be 0.74 ± 0.02 M using the titration method developed by Dacheux et al.[42,43] The thorium chloride concentrated solution was obtained by dissolving thorium nitrate hydrate ($Th(NO_3)_4 \cdot 4-5H_2O$) in 8 M HCl.[44] Several cycles of alternate evaporation and dissolution in 8 M hydrochloric acid were undertaken until all traces of nitrates were eliminated. The final thorium concentration was estimated to be 0.55 ± 0.02 M.

Synthesis of $Th_{1-x}U_xSiO_4$ solid solutions was carried out by adapting the protocol already described by Pointeau et al. for the preparation of coffinite.[25] In order to prevent any oxidation of U(IV) to U(VI), the whole procedure was performed in an inert glovebox flushed by argon (guaranteeing less than 1 ppm O_2) instead of the reducing atmosphere (N_2 − 5% H_2) used by Pointeau et al.[25]

Stoichiometric amounts of thorium and uranium chloride were first diluted in 5 mL of deionized water in order to obtain 1 mmol of a starting solution with the desired x stoichiometric ratio ($0 \le x \le 0.8$). This latter was added dropwise to an aqueous solution containing 1.03 mmol of Na_2SiO_3, resulting in a 3% molar excess in silicate compared to cations.

Table 1. Precipitation Yields Determined for Th, U, and Si from ICP-AES Measurements of the Supernatants

x (calcd)	thorium	uranium	silicon
0.3	>99.9	93.0 ± 2.7	97.8 ± 1.6
0.5	>99.9	95.2 ± 1.7	95.5 ± 1.7
0.8	>99.9	98.4 ± 1.8	94.4 ± 1.6

The pH was then raised to close to 9 by adding 8 M NaOH, resulting in the precipitation of a gelatinous phase, then finally buffered to 8.6 ± 0.1 by adding $NaHCO_3$.

The resulting gel probably consisted of (Th,U)-silica colloids.[45] It was poured in a PTFE-lined Parr instruments autoclave (maximum volume of 23 mL), then heated under hydrothermal conditions at 250 °C for 24 h. The precipitate obtained was separated from the supernatant by centrifugation, washed three times with deionized water and ethanol, then finally dried overnight at 60 °C in an oven.

ICP-AES analyses were then performed on the supernatants by the means of a Spectro Arcos EOP device in order to evaluate the thorium, uranium, and silicon recovery yields during the precipitation. The apparatus was calibrated with SPEX standard solutions diluted to concentrations ranging from 0.1 to 5 $mg \cdot L^{-1}$. The emission bands considered were located at λ = 279.39, 385.96, and 409.01 nm for uranium; at 274.72, 283.23, 283.73, and 401.91 nm for thorium; and at 152.67, 212.41, 251.61, and 288.16 nm for silicon.

Initial supernatant and washing solutions were poured together and adjusted to a global volume of 50 mL by adding deionized water. An aliquot of 0.5 mL was then removed and diluted to a final volume of 10 mL before ICP-AES measurement. From the results gathered in Table 1, the precipitation of thorium appeared to be systematically quantitative since its concentration in the supernatant was always found below the detection limit of the apparatus (i.e., ∼0.05 ppm). On this basis, less than 2.10^{-4} mmol remained in the supernatant, leading to a precipitation yield over 99.9%.

On the other hand, uranium precipitation did not appear to be quantitative, especially for the lower x values, as a probable consequence of the presence of small amounts of uranium(VI) in the starting solution. Nevertheless, uranium precipitation yield was found to increase with its starting amount in solution and reached up to 99.6% for x = 0.8. An opposite tendency was noted for silicon, which appeared to be underincorporated for high uranium amounts. As the cation/SiO_4 mole ratio was not significantly affected by the x value (and kept equal to 1.03), the precipitation yield seemed to be controlled by the uranium concentration. Moreover, the lower precipitation yield measured for silicon when considering the higher x values fitted well with the persistent difficulties reported in the literature for preparing pure coffinite without any simultaneous formation of UO_2 dioxide as a secondary phase.

2.2. Characterization Techniques. *Powder X-Ray Diffraction.* XRD diagrams were obtained by means of a Bruker D8 diffractometer equipped with a Lynx-eye detector adopting the Bragg−Brentano geometry and using Cu $K\alpha_{1,2}$ radiation (λ = 1.54184 Å). XRD patterns were recorded at room temperature in the $5° \le 2\theta \le 100°$ range, with a step size of $\Delta(2\theta) = 0.01°$ and a total counting time of 4 h. Pure silicon was measured under the same conditions and used as standard to extract the instrumental function. All powder patterns were refined with the Rietveld method using the Thomson−Cox−Hastings Pseudo Voigt convoluted with an axial divergence asymmetry function[46] with the Fullprof_Suite program.[47] On the one hand, eight profile and three structural parameters were refined for silicate phases, including a broadening effect by an anisotropic size model, preferred orientation, and thermal effect. On the other hand, only five profile and two structural parameters were considered for oxide phases due to their $m\bar{3}m$ Laue group.

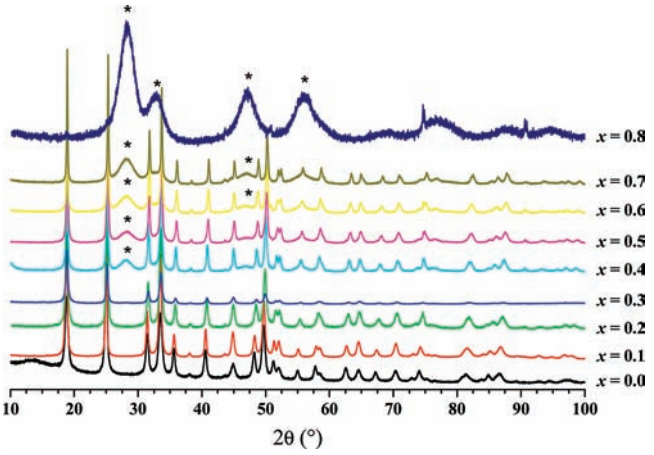

Figure 1. XRD patterns of uranothorite solid solutions with various chemical compositions. The main XRD lines of additional $Th_{1-y}U_yO_2$ oxide phase are pointed out by asterisks.

Table 2. Results of X-EDS Analyses Obtained for $Th_{1-x}U_xSiO_4$ Uranothorite Solid Solutions

x (calculated)	Th (atom %)	U (atom %)	An(IV)/Si	x (experimental)
0.1	15.1 ± 0.2	1.5 ± 0.1	0.99 ± 0.02	0.10 ± 0.01
0.2	13.8 ± 0.2	2.8 ± 0.2	1.00 ± 0.04	0.17 ± 0.07
0.3	13.0 ± 0.2	4.2 ± 0.2	1.07 ± 0.02	0.24 ± 0.01
0.4	11.3 ± 0.3	5.7 ± 0.5	1.04 ± 0.08	0.33 ± 0.02
0.5	9.8 ± 0.6	7.0 ± 0.7	1.02 ± 0.05	0.42 ± 0.03
0.6	9.5 ± 0.7	7.2 ± 0.7	1.01 ± 0.03	0.43 ± 0.04
0.7	6.4 ± 0.6	10.0 ± 0.7	0.98 ± 0.05	0.61 ± 0.04
0.8	No silicate formed after 24 hours			

Scanning Electron Microscopy. SEM observations were directly conducted on small powder samples without prior preparation such as metallization, using a FEI Quanta 200 electronic microscope, equipped either with an Everhart−Thornley Detector (ETD) or a Back-Scaterred Electron Detector (BSED), under high vacuum conditions with a very low accelerating voltage (2−3.1 kV). These conditions were chosen in order to create a beam deceleration effect that led to high resolution images.

X-Ray Energy Dispersive Spectroscopy. X-EDS analyses were performed using the Bruker AXS X-Flash 5010 detector coupled to the SEM device. In order to determine quantitatively the elementary atomic percentages as well as the mole ratios, the powders were first embedded in an epoxy resin. The surface of the sample was then polished to reach an optical grade and metalized by carbon deposition. Experimental data were finally collected from 30 different points by considering ThO_2, UO_2, and albite ($NaAlSi_3O_8$) as standards for quantitative measurements.

3. RESULTS AND DISCUSSION

3.1. Characterization of Uranothorite Solid Solutions. The qualitative analysis of the XRD patterns (Figure 1) revealed the formation of a two-phase system. The first phase corresponded to the expected thorium−uranium(IV) mixed silicate ($Th_{1-x}U_xSiO_4$) and exhibited all of the characteristic XRD lines of the tetragonal $I4_1/amd$ zircon-type structure previously reported for $ThSiO_4$,[48,49] $USiO_4$,[25] and other tetravalent actinide (Pu, Np, Am) silicates.[50] In this structural arrangement, the actinide is surrounded by eight oxygen atoms with two sets of four equal An−O distances. The resulting AnO_8 polyhedra share an edge with the SiO_4 tetrahedra to form chains along the c axis.

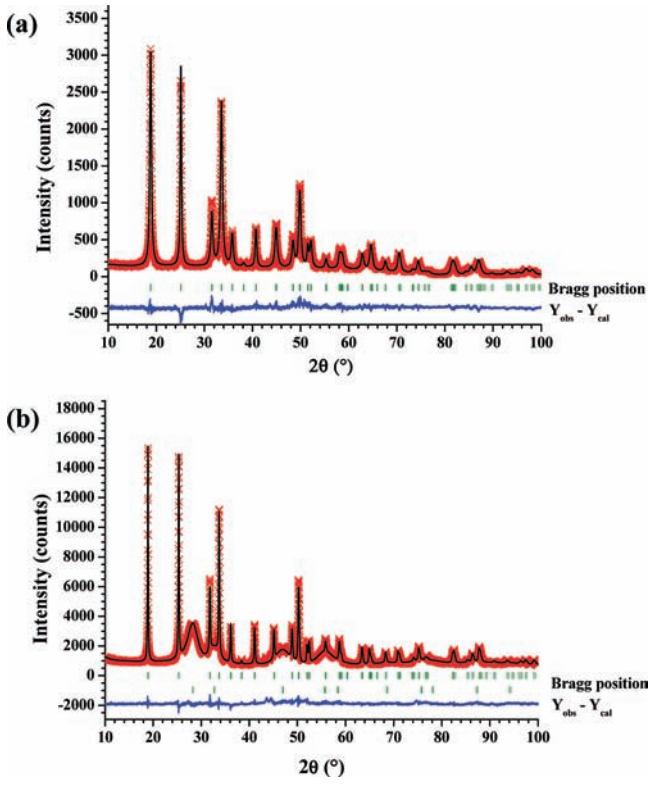

Figure 2. Rietveld plot obtained for $Th_{0.83}U_{0.17}SiO_4$ (a) and $Th_{0.39}U_{0.61}SiO_4$ (b) samples. Solid line stands for calculated data.

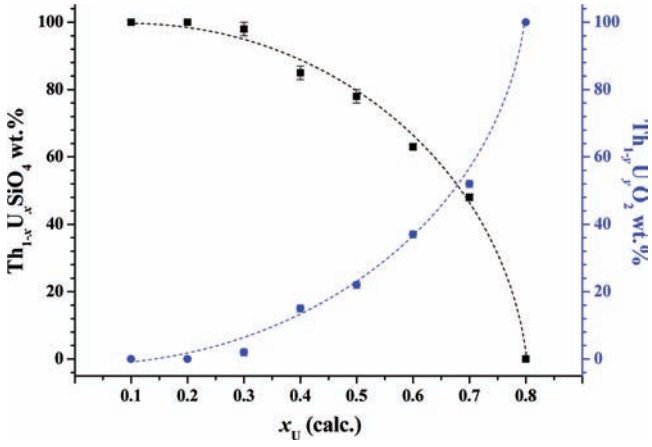

Figure 3. Variation of the weight contents of $Th_{1-x}U_xSiO_4$ and $Th_{1-y}U_yO_2$ phases versus expected uranium mole loading, x_U.

The second phase fitted well with the fluorite-type structure ($Fm\bar{3}m$ space group) associated with thorium−uranium(IV) mixed dioxides ($Th_{1-y}U_yO_2$).[51,52] The formation of such a secondary phase was not surprising since the presence of oxide phases associated with thorium−uranium(IV) silicates was frequently described in ore deposits[53,54] and was one among the causes of the late discovery of coffinite.[8] Nevertheless, the reflections associated with $Th_{1-y}U_yO_2$ appeared wide and/or weak in our system, which suggested that the dioxide phase was probably nanosized or poorly crystallized.

dx.doi.org/10.1021/ic2016758 |*Inorg. Chem.* 2011, 50, 11117–11126

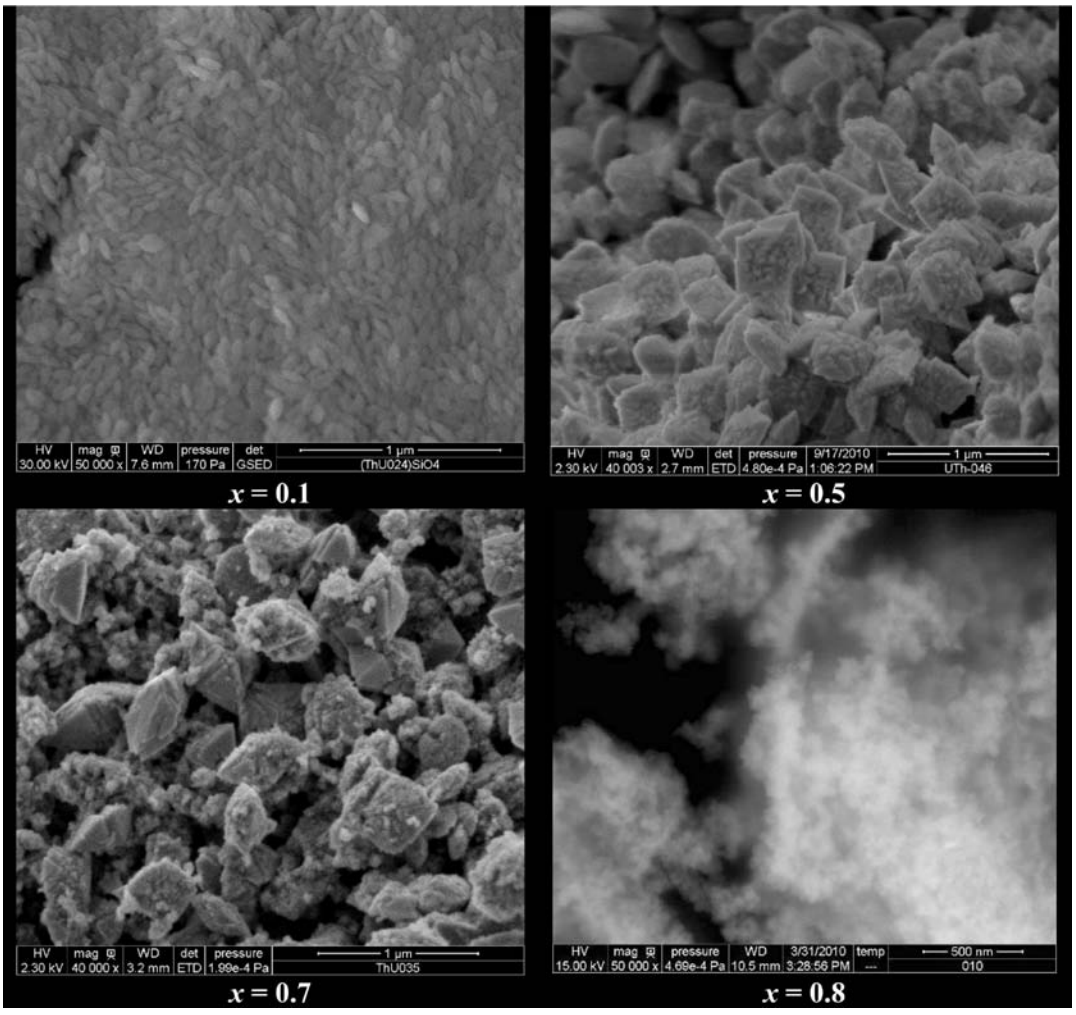

Figure 4. SEM micrographs of the systems obtained during the preparation of $Th_{1-x}U_xSiO_4$ uranothorite solid solutions.

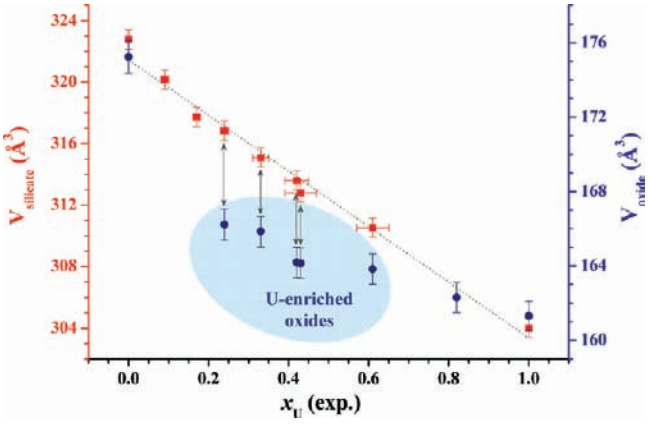

Figure 5. Refined unit cell volumes of $Th_{1-x}U_xSiO_4$ (■) and $Th_{1-y}U_yO_2$ (●) phase versus expected x value.

Also, no XRD line related to uranyl-bearing phases such as $(UO_2)_2(SiO_4)\cdot nH_2O$ soddyite,[55] $[(UO_2)_8O_2(OH)_{12}]\cdot 12H_2O$ schoepite,[56] or $Na(UO_2)(SiO_3OH)\cdot 1.5H_2O$ Na-boltwoodite[57] was detected during our experiments. On this basis, the operating conditions set up for the preparation of uranothorite solid solutions appeared to efficiently maintain the tetrapositive state of uranium in the reacting media during the synthesis since no U(VI) is expected to be incorporated in the $Th_{1-x}U_xSiO_4$ phase.[58]

Finally, it is also important to note that no other silicate-based phase was detected from the XRD experiments. On the basis of the stoichiometry of the starting reagents and on the recovery yields measured after precipitation, one should expect the formation of a Si-enriched compound to reach the quantitative precipitation of silicon. Under these conditions, the more likely option lied in the precipitation of amorphous and/or gelatinous SiO_2 jointly with that of uranothorite and thorium−uranium-(IV) oxide solid solutions. Indeed, the formation of silica was already observed previously in mineral assemblies,[9] during the synthesis of various zircon-type compounds, and in the Th−U−SiO_4 system.[39] The formation of such a phase was checked during our study through μ-Raman spectroscopy where the characteristic $\nu_S(SiO_2)$ vibration mode[59] was observed around 480 cm^{-1}.

All of the data collected (Table 2) were consistent with the formation of a uranothorite solid solution with average (Th+U)/SiO_4 mole ratio values close to 1. The slight deviations observed in several samples could be linked to the presence of the additional oxide-based phase in the analyzed zone or to the small

dx.doi.org/10.1021/ic2016758 |*Inorg. Chem.* 2011, 50, 11117–11126

Table 3. Refined Unit Cell Parameters of Uranothorite Solid Solutions and Oxide Side Products[a]

	$Th_{1-x}U_xSiO_4$ silicate				$Th_{1-y}U_yO_2$ dioxide			
x (calcd)	x (exptl)	a (Å)	c (Å)	V (Å^3)	a (Å)	V (Å^3)	y (calcd)[b]	ref
0.0		*7.1328(2)*	*6.3188(2)*	*321.48(2)*				49
					5.595(1)	*175.2(9)*		52
0.0	0	7.148(1)	6.309(1)	322.8(7)				
0.1	0.09(1)	7.119(1)	6.317(1)	320.2(6)				
0.2	0.17(1)	7.095(1)	6.320(1)	317.7(5)				
0.3	0.24(1)	7.085(2)	6.310(1)	316.8(7)	5.498(2)	166.2(7)	0.65	
0.4	0.33(2)	7.069(3)	6.305(1)	315.1(6)	5.494(3)	165.8(4)	0.68	
0.5	0.42(3)	7.056(1)	6.299(1)	313.6 (7)	5.475(4)	164.2(8)	0.79	
0.6	0.43(4)	7.049(1)	6.296(1)	312.8 (6)	5.475(2)	164.1(7)	0.80	
0.7	0.61(4)	7.028(1)	6.286(1)	310.5(6)	5.471(6)	163.8(8)	0.82	
0.8					5.455(1)	162.3(3)	0.92	
1.0		*6.995(1)*	*6.262(1)*	304.1(6)				25
					5.443(1)	*161.3(8)*		*this work*

[a] The rows in italics present the reference values used for oxide and silicate end members. [b] Interpolated from unit cell volume of ThO_2 and UO_2.

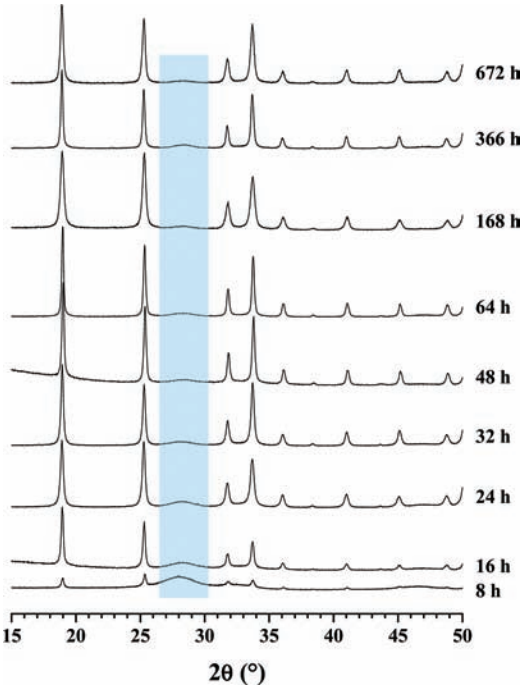

Figure 6. Evolution of the XRD pattern of the systems obtained for x = 0.5 versus the heating time.

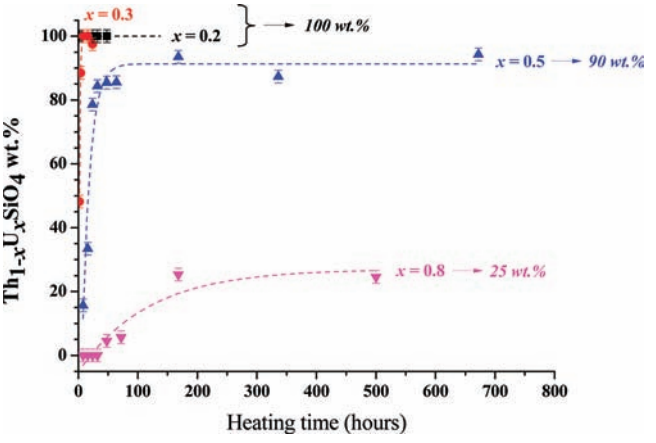

Figure 7. Evolution of $Th_{1-x}U_xSiO_4$ wt % versus heating time obtained for x = 0.2 (■), 0.3 (●), 0.5 (▲), and 0.8 (▼) (T = 250 °C). The maximum amount of uranothorite obtained for each composition is indicated on the graph.

size of the particle analyzed, which could lead to small bias in the measurements.

Furthermore, uranium content was generally found to be lower than that initially expected in the prepared samples for x > 0.2. This uranium depletion could arise partly from the small fraction of uranyl present in the starting solution, which remained in the supernatant all during the synthesis. Nevertheless, it mainly came from the formation of the thorium−uranium(IV) dioxide secondary phase evidenced from XRD, which became more and more important with increasing uranium mole loading x.

3.2. Influence of the Uranium Content on the Synthesis of Uranothorite Solid Solutions. The Rietveld refinement of the XRD patterns obtained from the sample series was performed by considering both phases, i.e., thorium−uranium(IV) mixed silicate and thorium−uranium(IV) mixed dioxide. Under these conditions, a good agreement was observed between experimental and calculated data whatever the sample prepared: indeed, both systems composed by one (such as $Th_{0.83}U_{0.17}SiO_4$, Figure 2a) or two phases (e.g., $Th_{0.39}U_{0.61}SiO_4$, Figure 2b) led systematically to R_{Bragg}, R_F, R_P, and R_{WP} reliability factors in the 5−8% range (cited agreements were given by Fullprof[47] after the Rietveld refinement: R_P and R_{WP} are respectively profile and weight profile factors; R_{Bragg} and R_F depend on the intensities and structure factor). The refinement of XRD patterns also led to quantification of the amount of the different phases present in the sample (Figure 3, precise data supplied as Supporting Information).

Three distinct domains were observed when studying the variation of silicate and dioxide amounts versus the initial chemical composition. For low uranium mole loadings ($0 \leq x \leq 0.3$), only thorium−uranium(IV) mixed silicate was detected by XRD, meaning that less than 1 wt % of additional dioxide phase was present in the sample. From x = 0.3 to 0.7, the

dx.doi.org/10.1021/ic2016758 |Inorg. Chem. 2011, 50, 11117–11126

synthesis process led to the coexistence of both oxide and silicate phases. Nevertheless, the amount of thorium−uranium(IV) dioxide in the mixture appeared to continuously increase with the uranium content in the starting solution, then became the major phase for $x = 0.7$. For higher uranium mole loadings, this tendency was exhausted, then led to the formation of thorium−uranium(IV) dioxide as the only crystalline phase for $x = 0.8$. As the recovery yield of uranium was a maximum for $x = 0.8$, the uranium precipitation appeared to be more important in the dioxide phase than in the uranothorite solid solution for our operating conditions. Moreover, the absence of silicate phases for higher uranium contents reflected the persisting difficulties in easily obtaining a pure uranium(IV) silicate phase, as already mentioned in the literature.

SEM micrographs (Figure 4) confirmed the presence of two distinct phases in the samples prepared. On the one hand, mixed silicates consisted of nanometric crystallites assembled into bipyramidal aggregates, as already observed for natural samples of uranium- and thorium-bearing zircon.[60] This morphology corresponds to the {111} bipyramid with no proof of the presence of the {110} form. The size of such aggregates was found to increase with the uranium content in the sample. Indeed, statistic measurements obtained on at least 30 grains led to average sizes increasing from 120 ± 20 nm ($x = 0.1$) to 330 ± 70 nm ($x = 0.5$) and then to 450 ± 60 nm ($x = 0.7$). On the other hand, the size of the crystallites constituting the grains (i.e., domain of coherence length), determined during the Rietveld refinement of XRD data, did not follow the same trend since it was systematically found between 10 and 30 nm, whatever the initial composition considered. Nevertheless, it allowed for confirmation of the polycrystalline nature of the uranothorite grains evidenced during these observations.

On the other hand, the secondary thorium−uranium(IV) dioxide phase appeared as spheres of about 2−5 nm scattered onto the silicate crystals. As expected from the XRD data, the occurrence of thorium−uranium(IV) dioxide nanoparticles increased significantly with the uranium mole content in the sample to become the only phase obtained for $x \geq 0.8$ under the operating conditions considered, i.e., $T = 250$ °C and $t = 24$ h. Moreover, for this initial composition, nanostructured $Th_{1-y}U_yO_2$ particles seemed to be embedded in a gelatinous layer, which could be associated with the precipitation of amorphous silica, already suggested from the recovery yields determined through ICP-AES measurements.

3.3. Variation of the Unit Cell Parameters versus the Uranium Mole Loading. Correlatively to the quantification of the phases formed during the hydrothermal process, the Rietveld refinement of the XRD patterns led to the evaluation of the lattice parameters of $Th_{1-x}U_xSiO_4$ uranothorite compounds ($I4_1/amd$ space group). The variation of the unit cell volume as a function of the uranium mole loading in the silicate phase (Figure 5) showed a regular decrease according to Vegard's law, in good agreement with the ioinic radii of Th^{4+} and U^{4+} in the 8-fold coordination (1.05 Å and 1.00 Å, respectively).[61] The linear variation of the unit cell parameters (Table 3) then attested to the existence of a complete solid solution between thorite and coffinite end members. Also, it confirmed the homogeneity in the chemical composition of the uranothorite samples prepared and precluded the coexistence of multiple silicated phases. On this basis, the preparation of uranothorite solid solutions with $x > 0.7$ should be achievable from a thermodynamic point of view. The results obtained under our operating conditions

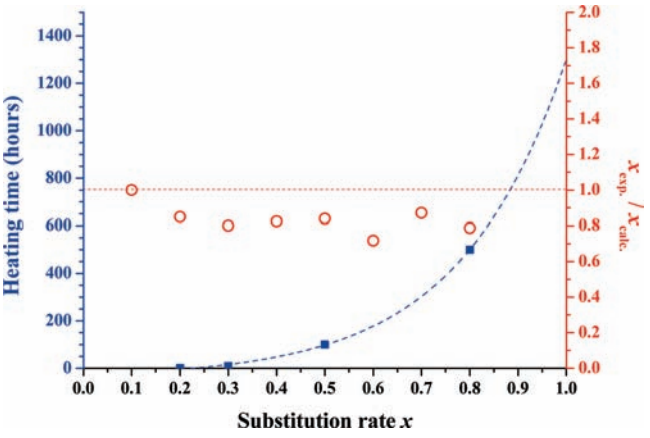

Figure 8. Variation of the heating time required to reach the maximum amount of $Th_{1-x}U_xSiO_4$ solid solution versus x_{calcd} (blue) and corresponding x_{exptl}/x_{calcd} ratio (red).

Table 4. Refined Unit Cell Volumes of Uranothorite Solid Solutions versus Heating Time at 250°C

	unit cell volume (Å^3)			
heating time (hours)	$x = 0.2$	$x = 0.3$	$x = 0.5$	$x = 0.8$
interpolated[a]	318.0	316.3	312.8	307.6
2	317.6(2)	316.9(2)		
4	317.3(2)	316.9(1)		
6	316.8(1)			
8	317.2(1)	315.1(1)	313.2(2)	
16	317.7(1)	315.4(1)	313.5(2)	
24	317.7(1)	317.1(3)	313.6(1)	
32	317.5(1)		313.1(2)	308.7(2)
48	317.4(1)		312.6(1)	
64			312.7(1)	
72				309.7(3)
168			312.3(2)	309.9(1)
336			312.9(1)	

[a] Values interpolated from $ThSiO_4$[49] and $USiO_4$[25] unit cell volumes.

(i.e., formation of pure thorium−uranium(IV) dioxide phases for $x \geq 0.8$) then probably resulted from a kinetic hindering in the precipitation mechanism.

The Rietveld refinement also allowed for a determination of the unit cell parameter of the $Th_{1-y}U_yO_2$ phase (Table 3). As the existence of a complete solid solution was previously described in the literature in the ThO_2-UO_2 binary system,[62−64] the thorium substitution rate in the dioxide phase (y) was estimated by interpolation of the data obtained in this work with that of pure ThO_2 and intermediate $Th_{1-y}U_yO_2$ solid solutions.[52] Since the unit cell parameters of the pure UO_2 end member were reported to strongly depend on the U/O stoichiometry and on the refinement method, a homemade reference was prepared by firing $U(C_2O_4)_2 \cdot 2H_2O$ at $T = 500$ °C.[65,66]

As expected from the precipitation yields and the stoichiometry of the silicate phase, $Th_{1-y}U_yO_2$ solid solution was found to be strongly uranium-enriched ($0.6 \leq y \leq 0.8$). On this basis, the quantitative precipitation of uranium for high uranium mole contents could be linked to the formation of the U-enriched

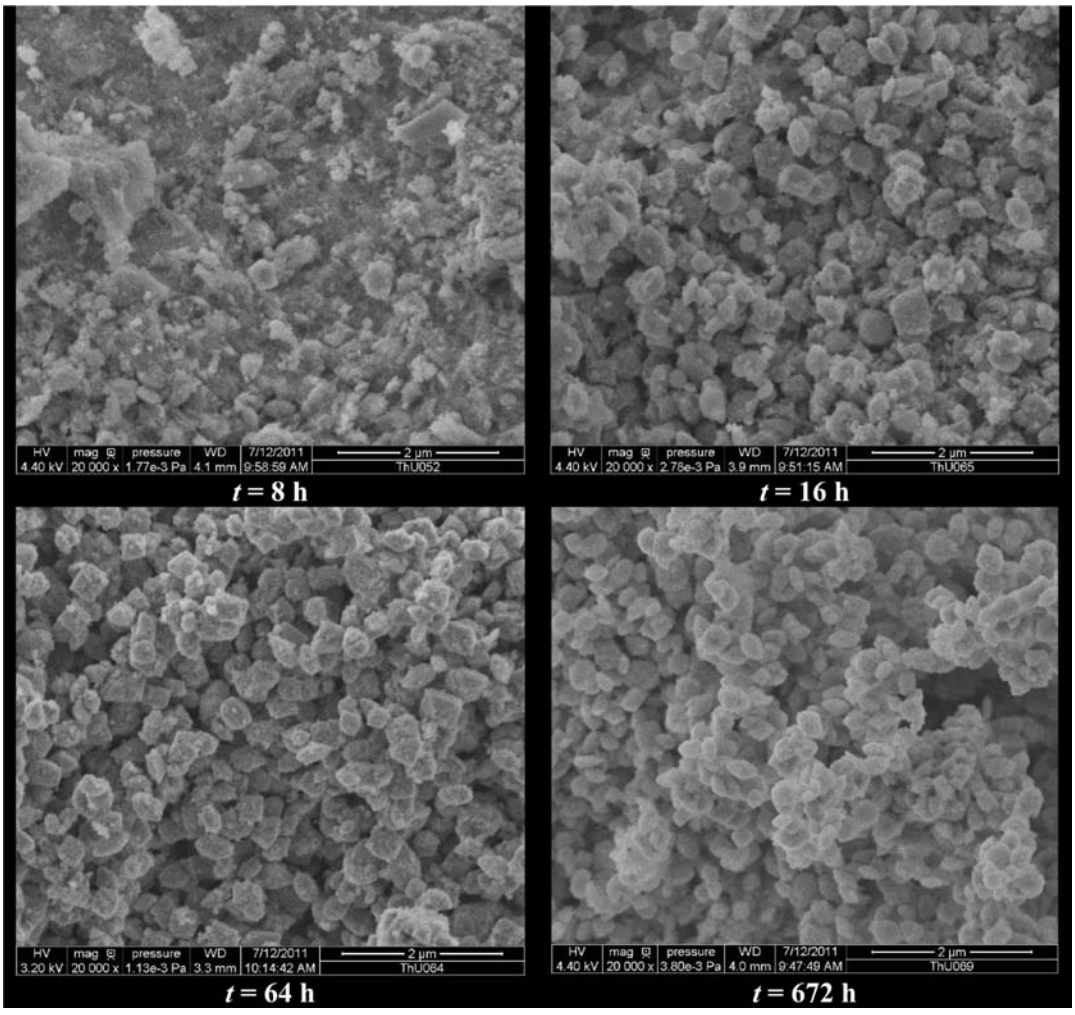

Figure 9. SEM observations of the uranothorite samples obtained for $x = 0.5$ after 8, 16, 64, and 672 h of heating at 250 °C.

oxide phase. The preferential formation of $Th_{1-y}U_yO_2$ and SiO_2 instead of $Th_{1-x}U_xSiO_4$ solid solutions under our operating conditions for high uranium mole loadings fitted well with the results obtained for coffinite.[67] Also, it could be in favor of some chemical processes based on the initial formation of $Th_{1-y}U_yO_2$ solid solutions then on a coffinitization-like reaction leading from the $Th_{1-y}U_yO_2 + SiO_2$ mixture to $Th_{1-x}U_xSiO_4$ solid solution as already described in geological media.[68,69]

3.4. Understanding of the Uranothorite Kinetics of Formation. Since the operating conditions developed for the synthesis of uranothorite solid solutions failed to prepare pure and single phase samples for $x > 0.3$, the kinetics impact was evaluated by varying the heating duration of the hydrothermal treatment ($T = 250$ °C). As an example, the XRD pattern of the sample prepared for $x = 0.5$ was recorded for various heating times ranging from 8 to 672 h (Figure 6). From these data, the intensity of the XRD lines associated with the oxide phase (estimated from their height) was found to decrease significantly when increasing the holding time for such hydrothermal conditions which corresponded to an increase of the silicate amount in the two-phase systems obtained.

This phenomenon was confirmed through the phase quantification performed by Rietveld refinement (Figure 7): as an example, for $x = 0.5$, the uranothorite weight percent varied from 15% after 8 h of heat treatment to about 95% after 672 h. Under these conditions, the reaction mechanism leading to uranothorite seems to be initiated by the nucleation of $Th_{1-y}U_yO_2$ nanoparticles and of amorphous and/or colloidal silica. The formation of $Th_{1-x}U_xSiO_4$ solid solutions is then obtained through a dissolution/precipitation process.

On this basis, the mixture of oxide phases initially present in the reacting media appeared less stable than the $Th_{1-x}U_xSiO_4$ solid solution itself under our operating conditions. Such observation appeared in good agreement with the data calculated by Fleche.[13] It also fitted well with the geological observations which reported the preferential precipitation of thorium and uranium as $Th_{1-x}U_xSiO_4$ solid solutions in silicate-based media.[7,70]

Moreover, the variation of the uranothorite weight percent was found to empirically follow a reverse exponential function of time, already described in the literature for the precipitation of silica from silicon oligomers and nanocolloids.[71,72] Under these conditions, the amount of silicate in the system strongly increased during the first 50 h of heating, then reached a plateau. A similar tendency was observed whatever the chemical composition of the starting mixture considered (Figure 7). Nevertheless, the hydrothermal time required to obtain an optimal quantity of silicate as well as its maximal amount was found to be strongly dependent on the composition of the starting mixture. Indeed,

dx.doi.org/10.1021/ic2016758 |*Inorg. Chem.* 2011, 50, 11117–11126

while $Th_{1-x}U_xSiO_4$ solid solutions appeared to be single-phase after a few hours for $0 \leq x \leq 0.3$, the formation of the uranothorite solid solution was only observed after 48 h of heating for $x = 0.8$, while its weight content only reached ~25 wt %. Under these latter conditions, the rapid and preferential formation of the thorium−uranium(IV) dioxide phase was also correlated with the decrease of the silicon recovery yield at $t = 24$ h (Table 1).

These results suggest that, with the operating conditions considered:

(i) The formation of $USiO_4$ coffinite should only occur for very long heating times, i.e., probably more than several dozen days (Figure 8).

(ii) Only limited amounts of coffinite should be obtained, with the additional major presence of uranium dioxide.

It is also important to note that the chemical composition of the silicate phase obtained was almost constant whatever the heating duration considered. Indeed, the variation of the unit cell volume remained very weak (i.e., below 0.5%) when making the comparison to the reference value determined for $t = 24$ h (Table 4). Under these conditions, the total amount of uranium initially precipitated in the $Th_{1-y}U_yO_2$ nanophase did not appear to be incorporated in the final $Th_{1-x}U_xSiO_4$ solid solution. The depletion in uranium should then occur during the dissolution step of the dioxide through the partial oxidation of U(IV) as a uranyl molecular ion which was not incorporated into the uranothorite structure.[58] This was correlated to a slight decrease of the uranium precipitation yield when increasing the heating duration under hydrothermal conditions, indicating that uranium(VI) present in the supernatant did not precipitate under our operating conditions. Nevertheless, the relative amount of uranium finally incorporated into the uranothorite phase appeared to be barely constant in the composition range considered, the x_{exptl}/x_{calcd} mole ratio being systematically close to 0.8 for $x > 0.1$ (Figure 8).

The decrease of the U-enriched dioxide phase amount was also followed during the hydrothermal heat treatment at 250 °C by SEM observations performed on the system prepared for $x = 0.5$ (Figure 9). After 8 h of heating, the system appeared mainly composed of nanometric grains, assigned to the $Th_{1-y}U_yO_2$ phase, and to larger aggregates probably formed by amorphous silica. The $Th_{1-x}U_xSiO_4$ grains were thus not clearly observed, which agreed well with the low mass content determined under such conditions (about 15 wt %). Conversely, bipyramidal grains characteristic of zircon-type structures were systematically observed for longer heating times. Moreover, the occurrence of the $Th_{1-y}U_yO_2$ nanoparticles scattered onto the surface of uranothorite grains was found to decrease progressively to become almost invisible after 672 h. Also, it is worth noting that the grain size of $Th_{1-x}U_xSiO_4$ was not significantly affected by the heating duration. Indeed, whatever the heating time considered between 16 and 672 h, the bipyramidal grains were found between 100 and 300 nm in length. Simultaneously, no important increase of the crystallite size was evidenced from Rietveld refinements of XRD data collected for $x = 0.2$ (Table 5). Indeed, this latter was found to increase moderately from about 100 to 170 Å between 2 and 48 h of heat treatment.

Table 5. Evolution of the Refined Crystallite Size versus Heating Time ($T = 250$°C) for $Th_{0.8}U_{0.2}SiO_4$

heating time (h)	crystalite size (Å)	anisotropy (Å)	heating time (h)	crystalite size (Å)	anisotropy (Å)
2	94	±24	16	134	±21
4	128	±25	32	168	±28
6	142	±21	48	172	±25
8	146	±26			

4. CONCLUSION

$Th_{1-x}U_xSiO_4$ uranothorite solid solutions were prepared under hydrothermal conditions for $0 \leq x \leq 0.8$ ($T = 250$ °C). From XRD data, a complete solid solution was formed for $x \leq 0.8$ while additional U-enriched $(Th,U)O_2$ dioxide and amorphous silica were systematically detected for the highest uranium mole loadings. Particular attention was then paid to the influence of kinetics parameters on the precipitation mechanism. Since the

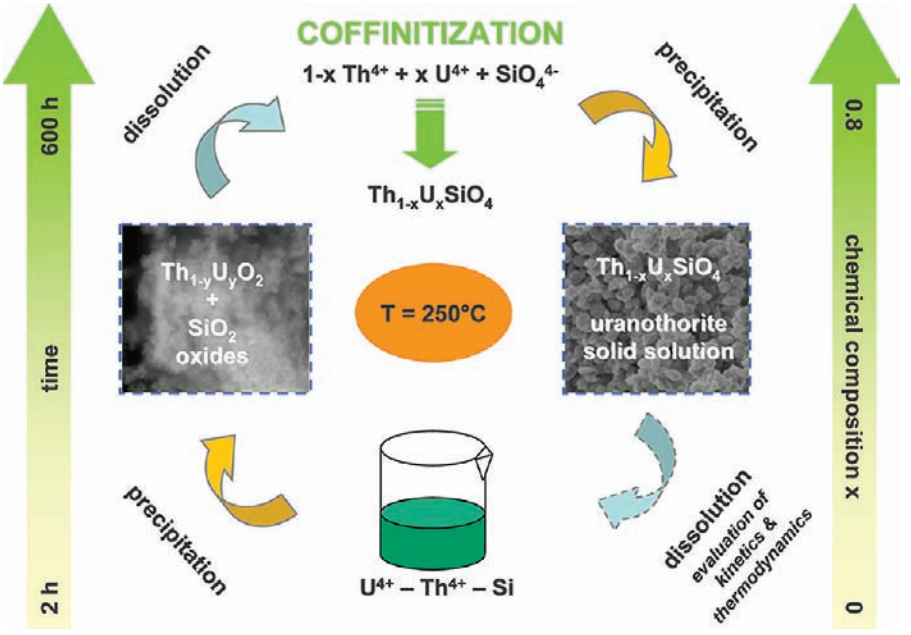

Figure 10. Schematic representation of the mechanism proposed for the formation of $Th_{1-x}U_xSiO_4$ uranothorite solid solutions.

dx.doi.org/10.1021/ic2016758 |Inorg. Chem. 2011, 50, 11117–11126

amount of silicate compound in the polyphase system was found to increase with heating time to reach a maximum value depending on the x mole ratio, the precipitation of oxide phases was proposed as a first step in the mechanism of formation of $Th_{1-x}U_xSiO_4$ compounds (Figure 10). Their transformation into uranothorite solid solutions is then expected through a dissolution/reprecipitation process close to that reported as coffinitization. Nevertheless, this reaction was frequently associated with a loss of about 20% of the initial uranium, probably due to the partial oxidization of U(IV) into uranyl.

Also, the holding time required to obtain uranothorite strongly increased with the uranium mole ratio. Consequently, the formation of coffinite, even if thermodynamically achievable, should only occur for heating times exceeding several dozens of days. The difficulties in synthesizing coffinite reported over the decades are thus probably mainly linked to kinetics constraints associated with the reaction of coffinitization. Such kinetic hindering then makes the pure coffinite hardly obtainable on the laboratory time-scale but allows its observation in natural ores.

As the final aim of this work deals with the determination of thermodynamic data, the preparation of pure $Th_{1-x}U_xSiO_4$ is now under study. Multiparametric studies of the dissolution kinetics of $Th_{1-x}U_xSiO_4$ solid solutions are also in progress.

■ ASSOCIATED CONTENT

Supporting Information. Refined weight amounts for $Th_{1-x}U_xSiO_4$ and $Th_{1-y}U_yO_2$ phases in the obtained mixtures. This material is available free of charge via the Internet at http://pubs.acs.org.

■ AUTHOR INFORMATION

Corresponding Author

*Phone: + 33 4 66 33 92 08. Fax: + 33 4 66 79 76 11. E-mail: nicolas.clavier@icsm.fr.

■ ACKNOWLEDGMENT

The authors are grateful to the GUTEC research group (Geology of Uranium and Thorium: Extraction, Conversion) included in the PACEN program of CNRS for its financial support.

■ REFERENCES

(1) French law no. 2006−739, 28 June 2006. http://www.assemblee-nationale.fr/12/dossiers/gestion_dechets_radioactifs_programme.asp (accessed September 2011).

(2) Voizard, P.; Mayer, S.; Ouzounian, G. *Proceedings of the 11th International Conference on Environmental Remediation and Radioactive Waste Management ICEM2007*; ASME: New York, 2009, 125.

(3) Gaucher, E.; Blanc, P.; Bardot, F.; Braibant, G.; Buschaert, S.; Crouzet, C.; Gautier, A.; Girard, J. P.; Jacquot, E.; Lassin, A.; Negrel, G.; Tournassat, C.; Vinsot, A.; Altmann, S. *C.R. Geosci.* **2006**, *338*, 917–930.

(4) Stieff, L. R.; Stern, T. W.; Sherwood, A. M. *Science* **1955**, *121*, 608–609.

(5) Utsunomiya, S.; Deditius, A. P.; Pointeau, V.; Ewing, R. C. *Geochim. Cosmochim. Acta* **2008**, *72*, 968–968.

(6) Janeczek, J.; Ewing, R. C. *J. Nucl. Mater.* **1992**, *190*, 157–173.

(7) Cuney, M. *Econ. Geol.* **1978**, *73*, 1567–1610.

(8) Ludwig, K. R.; Grauch, R. I. *Econ. Geol.* **1980**, *75*, 296–302.

(9) Förster, H. J. *Lithos* **2006**, *88*, 35–55.

(10) Langmuir, D. *Geochim. Cosmochim. Acta* **1978**, *42*, 547–569.

(11) Langmuir, D. In *Aqueous environmental geochemistry*; Prentice Hall, New Jersey, 1997.

(12) Guillaumont, R.; Fanghanel, T.; Fuger, J.; Grenthe, I.; Neck, V.; Palmer, D. A.; Rand, M. H. In *Update on the chemical thermodynamics of uranium, neptunium, plutonium, americium and technicium*; NEA, OECD: Moulineaux, France, 2003.

(13) Fleche, J. L. *Phys. Rev. B* **2002**, *65*, 245116.

(14) Valéro, R.; Durand, B.; Guth, J. L.; Chopin, T. *Micropor. Mesopor. Mater.* **1999**, *29*, 311–318.

(15) Alarcon, J. *J. Eur. Ceram. Soc.* **2000**, *20*, 1749–1758.

(16) Veytizou, C.; Quinson, J. F.; Jorand, Y. *J. Eur. Ceram. Soc.* **2002**, *22*, 2901–2909.

(17) Fuhrmann, J.; Pickardt, J. *Z. Anorg. Allg. Chem.* **1986**, *532*, 171–174.

(18) Kanno, Y. *J. Mater. Sci. Lett.* **1993**, *12*, 1807–1809.

(19) Frondel, C.; Collette, R. L. *Am. Mineral.* **1957**, *42*, 759–765.

(20) Fuchs, L. H. *Am. Mineral.* **1958**, *43*, 367–368.

(21) Sinha, D. P.; Prasad, R. *J. Inorg. Nucl. Chem.* **1973**, *35*, 2612–2614.

(22) Kamegashira, N. *J. Mater. Sci.* **1979**, *14*, 505–506.

(23) Fuchs, L. H.; Hoekstra, H. R. *Am. Mineral.* **1959**, *44*, 1057–1063.

(24) Mulak, J. *J. Solid State Chem.* **1977**, *21*, 117–126.

(25) Pointeau, V.; Deditius, A. P.; Miserque, F.; Renock, D.; Becker, U.; Zhang, J.; Clavier, N.; Dacheux, N.; Poinssot, C.; Ewing, R. C. *J. Nucl. Mater.* **2009**, *393*, 449–458.

(26) Pishva, F. In *Synthesis of uranium silicate*. Master Degree report, East Texas State University, Commerce, TX, 1991.

(27) Uziemblo, N. H.; Thomas, L. E.; Schoenlein, L. H.; Mastel, B.; Jenson, E. D. *Mater. Res. Soc. Symp. Proc.* **1987**, *84*, 161–171.

(28) Amme, M.; Renker, B.; Schmid, B.; Feth, M. P.; Bertagnolli, H.; Döbelin, W. *J. Nucl. Mater.* **2002**, *306*, 202–212.

(29) Robit, V. In *Etude des phases néoformées lors de la dissolution du combustible nucléaire en condition de stockage géologique : influence des ions silicates*, PhD Thesis, Université Paris-Sud-11, France, 2005.

(30) Zimmer, P. In *Etude expérimentale à huate pression et haute tempéarture du système ternaire UO2-ThO2-SiO2 en présence d'une phase fluide*, CREGU report n 12; CREGU: Nancy, France, 1986.

(31) Lian, J.; Zhang, J. M.; Pointeau, V.; Zhang, F. X.; Lang, M.; Lu, F. Y.; Poinssot, C.; Ewing, R. C. *J. Nucl. Mater.* **2009**, *393*, 481–486.

(32) Vitorge, P. In *Law of mass action for co-precipitation*, CEA report no. CEA-R-6193; CEA: Gif-sur-yvette Cedex, France, 2008 (http://www.vitorge.name/pierre/publis/08vit.pdf; accessed September 2011).

(33) Ifill, R. O.; Cooper, W. C.; Clark, A. H. *CIM Bull.* **1987**, *80*, 72–72.

(34) Lira, R.; Ripley, E. M. *Contrib. Mineral. Petr.* **1992**, *110*, 370–386.

(35) Sharma, G. S.; Purohit, R. K.; Roy, M.; Sengupta, B.; Singh, J. *J. Geol. Soc. Ind.* **2000**, *55*, 189–196.

(36) Pabst, A. *Am. Mineral.* **1951**, *36*, 557–562.

(37) Fuchs, L. H.; Gebert, E. *Am. Mineral.* **1958**, *43*, 243–248.

(38) Caruba, R.; Baumer, A.; Turco, G. *Geochim. Cosmochim. Acta* **1975**, *39*, 11–26.

(39) Ushakov, S. V.; Gong, W.; Yagovkina, M. M.; Helean, K. B.; Lutze, W.; Ewing, R. C. *Ceram. Trans.* **1999**, *93*, 357–363.

(40) Burakov, B. E.; Anderson, E. B.; Zamoryanskaya, M. V.; Yagovkina, M. A.; Strykanova, E. E.; Nikolaeva, E. V. *Mater. Res. Soc. Symp. Proc.* **2000**, *663*, 307–313.

(41) Geisler, T.; Burakov, B.; Yagovkina, M.; Garbuzov, V.; Zamoryanskaya, M.; Zirlin, V.; Nikolaeva, L. *J. Nucl. Mater.* **2005**, *336*, 22–30.

(42) Dacheux, N.; Brandel, V.; Genet, M. *New J. Chem.* **1995**, *19*, 15–25.

(43) Dacheux, N.; Brandel, V.; Genet, M. *New J. Chem.* **1995**, *19*, 1029–1036.

(44) Dacheux, N.; Brandel, V.; Genet, M.; Bak, K.; Berthier, C. *New J. Chem.* **1996**, *20*, 301–310.

(45) Dreissing, I.; Weiss, S.; Henning, C.; Bernhard, G.; Zanker, H. *Geochim. Cosmochim. Acta* **2011**, *75*, 352–367.

(46) Finger, L. W.; Cox, D. E.; Jephcoat, A. P. *J. App. Cryst.* **1994**, *27*, 892–900.

(47) Roisnel, T.; Rodriguez-Carvajal, J. In *WinPLOTR: A windows tool for powder diffraction pattern analysis*, Materials Science Forum, Trans. Tech. Publications: Switzerland, Vol. 378-381, 2001; pp 118-123.
(48) Taylor, M.; Ewing, R. C. *Trans. Am. Geophys. Union* **1975**, *56*, 1076–1076.
(49) Taylor, M.; Ewing, R. C. *Acta Crystallogr., Sect. B* **1978**, *34*, 1074–1079.
(50) Speer, J. A. *Rev. Miner.* **1980**, *5*, 113–135.
(51) Yang, J. H.; Kang, K. W.; Song, K. W.; Lee, C. B.; Jung, Y. H. *Nucl. Technol.* **2004**, *147*, 113–119.
(52) Hubert, S.; Purans, J.; Heisbourg, G.; Moisy, P.; Dacheux, N. *Inorg. Chem.* **2006**, *45*, 3887–3894.
(53) Fayek, M.; Janeczek, J.; Ewing, R. C. *Appl. Geochem.* **1997**, *12*, 549–565.
(54) Fayek, M.; Harrison, T. M.; Ewing, R. C.; Grove, M.; Coath, C. D. *Chem. Geol.* **2002**, *185*, 205–225.
(55) Forbes, T. Z.; Horan, P.; Devine, T.; McInnis, D.; Burns, P. C. *Am. Mineral.* **2011**, *96*, 202–206.
(56) Finch, R. J.; Hawthorne, F. C.; Ewing, R. C. *Can. Miner.* **1998**, *36*, 831–845.
(57) Burns, P. C. *Can. Miner.* **1998**, *36*, 1069–1075.
(58) Teterin, Y. A.; Utkin, I. O.; Melnikov, I. V.; Lebedev, A. M.; Teterin, A. Y.; Ivanov, K. E.; Nikitin, A. S.; Vukchevich, L. *J. Struct. Chem.* **2000**, *41*, 965–971.
(59) Sidorov, T. A. *Russ. J. Inorg. Chem.* **2007**, *52*, 1586–1594.
(60) Reiners, P. W. *Rev. Mineral. Geochem.* **2005**, *58*, 151–179.
(61) Shannon, R. D. *Acta Crystallogr., Sect. A* **1976**, *32*, 751–767.
(62) Kanno, M.; Kokubo, S.; Furuya, H. *J. Nucl. Sci. Technol.* **1982**, *19*, 956–958.
(63) Dash, S.; Parida, S. C.; Singh, Z.; Sen, B. K.; Venugopal, V. *J. Nucl. Mater.* **2009**, *393*, 267–281.
(64) Rousseau, G.; Fattahi, M.; Grambow, B.; Desgranges, L.; Boucher, F.; Ouvrard, G.; Millot, N.; Niepce, J. C. *J. Solid State Chem.* **2009**, *182*, 2591–2597.
(65) Bharadwaj, D. S.; Vasudeva Murthy, A. R. *Indian J. Chem.* **1964**, *12*, 391–396.
(66) Duvieubourg-Garela, L.; Vigier, N.; Abraham, F.; Grandjean, S. *J. Solid State Chem.* **2008**, *181*, 1899–1908.
(67) Robit-Pointeau, V.; Poinssot, C.; Vitorge, P.; Grambow, B.; Cui, D.; Spahiu, K.; Catalette, H. *Mater. Res. Soc. Symp. Proc.* **2006**, *932*, 489–492.
(68) Janeczek, J.; Ewing, R. C. *Mater. Res. Soc. Symp. Proc.* **1992**, *257*, 497–504.
(69) Philippe, S.; Lancelot, J. R.; Clauer, N.; Pacquet, A. *Can. J. Earth Sci.* **1993**, *30*, 720–730.
(70) Zacek, V.; Skoda, R.; Sulovsky, P. *J. Geol.* **2009**, *54*, 343–354.
(71) Icopini, G. A.; Brantley, S. L.; Heaney, P. J. *Geochim. Cosmochim. Acta* **2005**, *69*, 293–303.
(72) Conrad, C. F.; Icopini, G. A.; Yasuhara, H.; Bandstra, J. Z.; Brantley, S. L.; Heaney, P. J. *Geochim. Cosmochim. Acta* **2007**, *71*, 531–542.